



Contents lists available at ScienceDirect

Deep-Sea Research II

journal homepage: www.elsevier.com/locate/dsr2

Integrated stratigraphic reconstruction for the last 80 kyr in a deep sector of the Sardinia Channel (Western Mediterranean)

F. Budillon^{a,*}, F. Lirer^a, M. Iorio^a, P. Macrí^b, L. Sagnotti^b, M. Vallefucoco^a, L. Ferraro^a, S. Garziglia^c, S. Innangi^a, M. Sahabi^d, R. Tonielli^a

^a Istituto per l'Ambiente Marino Costiero, IAMC, Consiglio Nazionale delle Ricerche, Calata Porta di Massa 80, I-80133 Napoli, Italy

^b Istituto Nazionale di Geofisica e Vulcanologia, INGV, Via di Vigna Murata 605, I-00143 Rome, Italy

^c Géosciences-Azur, CNRS, BP 48, Fr-06235, Villefranche sur Mer, France

^d Faculté des Sciences, BP 20, 24000 El Jadida, Morocco

ARTICLE INFO

Article history:

Accepted 9 July 2008

Available online 7 November 2008

Keywords:

Integrated stratigraphy

Late Neogene marine record

Eco-bio-events

Reflectance 550 nm %

Sardinia Channel

Western Mediterranean

ABSTRACT

A quantitative analysis of planktonic foraminifera, coupled with petrophysical and paleomagnetic measurements and ¹⁴C-AMS calibrations, was carried out on a deep core recovered in the Sardinia Channel (Western Mediterranean Sea), during the CIESM Sub2 survey, providing an integrated stratigraphic time-framework over the last 80 kyr. Significant changes in the quantitative distribution of planktonic foraminifera allowed the identification of several eco-bioevents useful to accurately mark the boundaries of the eco-biozones widely recognized in the Western Mediterranean records and used for large-scale correlations. Namely, 10 eco-biozones were identified based on the relative abundance of selected climate-sensitive planktonic foraminiferal species. Sixteen codified eco-bioevents were correlated with Alboran Sea planktonic foraminiferal data and several climatic global events (Sapropel S1, Younger Dryas, Greenland Isotope Interstadial 1, Greenland Isotope Stadial 2, Heinrich event H1–H6) were recognized.

The eco-bioevents together with the ¹⁴C-AMS calibrations allowed us to define an accurate age model, spanning between 2 and 83 kyr. The reliability of the age model was confirmed by comparing the colour reflectance (550 nm%) data of the studied record with the astronomically tuned record from the Ionian Sea (ODP-Site 964). A mean sedimentation rate of about 7 cm/kyr included three turbidite event beds that were chronologically constrained within the relative low stand and regressive sea-level phases of MIS 4 and 3. The deep-sea sedimentary record includes a distinct tephra occurring at the base of the core that dates 78 ka cal. BP.

The paleomagnetic data provide a well-defined record of the characteristic remanent magnetization that may be used to reconstruct the geomagnetic paleosecular variation for the Mediterranean back to 83 kyr.

© 2008 Elsevier Ltd. All rights reserved.

1. Introduction

Since climate excursions recorded in Northern Hemisphere in the Greenland GISP and GRIP ice cores (GRIP members, 1993) over the last 100 kyr had more or less synchronous effects in the Mediterranean area, many researches have focused on Mediterranean marine cores, with the aim to detect their intensity and impact on the marine environment. During the last glacial period the Mediterranean region experienced rapid modifications in hydrographic conditions in response to fast climatic excursions, such as Heinrich (HE) and Dansgaard–Oeschger (D–O) Stadials

(cold) and Interstadials (warm) events (Heinrich, 1988; Dansgaard et al., 1993). In particular, Rohling et al. (1998) and Cacho et al. (1999, 2000) have proved that the millennial scale D–O and HE directly control the winds and precipitation system on the northern Mediterranean basin. Even during the Holocene the principal climatic events and oscillations of the northern Hemisphere have been clearly traceable in different sectors of the Mediterranean basin sedimentary records (Cacho et al., 1999, 2000, 2001; Rohling et al., 2002; Sprovieri et al., 2003, 2006; Perez-Folgado et al., 2003, 2004; Geraga et al., 2005).

A detailed outline of the paleo-environmental changes and their control on marine communities, calibrated by several independent proxies (tephra, sapropel, ¹⁴C geochronology), is now available for the Mediterranean area (Buccheri et al., 2002; Ducassou et al., 2007; Emeis et al., 2003; Narcisi and Vezzoli,

* Corresponding author. Tel.: +390 81 542 3839; fax: +390 81 542 3888.

E-mail address: francesca.budillon@iamc.cnr.it (F. Budillon).

1999; Lourens, 2004; Principato et al., 2003; Rohling et al., 2003; Sangiorgi et al., 2006; Sprovieri et al., 2003, 2006, and reference therein). Several codified eco-bioevents, if clearly detected in marine records, can be used as tie points to chronologically constrain the late Pleistocene–Holocene Mediterranean marine sequence. Nevertheless, even if many reference records are available from deep-sea sites, most of them span a short time interval and lack a high resolution detail of the paleo-environmental and paleo-ecological changes before 40 kyr. Recently, Perez-Folgado et al. (2003, 2004) carried out a high-resolution study of the ODP-Site 977, located in the western part of the Alboran Sea, and identified several planktonic foraminiferal eco-bioevents that occurred during the marine isotope stages (MIS) 1–5. These eco-bioevents represent the best tool to correlate deep marine records from different Mediterranean sites.

Many recent studies emphasize the challenge when studying deep-sea records to establish a reliable chronology, even for the deposition of turbidites (Walker, 1992; Beaudouin et al., 2004; Ducassou et al., 2007), and underline the utility to support conventional dating methodologies with different constraints. It is widely accepted that one of the main factors controlling and enhancing turbidite deposition along deep-sea fan is the regression and low stand of sea-level, whereas sea-level rise and highstand phases reduce terrigenous supply to deep-sea systems (Walker, 1992; Richards et al., 1998; Normark et al., 1998).

The CIESM core C08 is located at the mouth of the Bizerte Canyon in the Sentinelle Valley in a key position of paleoceanographic and geological significance (Fig. 1). The Sardinia Channel connects the Alboran to the Tyrrhenian Basin and offers a stratigraphic record with the potential to link the eco-stratigraphic and paleoceanographic observations between the Western, Central and Eastern Mediterranean late Pleistocene–Holocene

marine records (Perez-Folgado et al., 2004; Sbaifi et al., 2004; Geraga et al., 2005; Asioli et al., 2001; Ariztegui et al., 2000). In fact, a portion of the Modified Atlantic Water (MAW) coming from the Strait of Gibraltar (Bryden and Kinder, 1991), diverges from the part that enters the Eastern Mediterranean and flows through the Sardinia Channel into the Tyrrhenian Sea along the northern Sicilian coast (Millot, 1987), forming a secondary circulation gyre. The circulation system in this sector of the Tyrrhenian Sea is counter-clockwise, with the Levantine Intermediate Water (LIW) inflows lapping on the northern Sicilian coast and the outflow occurring along the eastern Sardinia coast (Pinardi and Masetti, 2000 and references therein).

The core site is also in a strategic position to check the efficiency of a submarine canyon in driving density flow to the deep-sea environment (see below), even if not directly connected to any emerged sector nor to continental shelf (Reading and Richards, 1994). Thus the possibility that such a type of canyon would form a fan can be evaluated, even verifying the significance and the timing of the turbidite deposition.

The aim of this study is to provide a record of integrated stratigraphic data spanning back to about 80 kyr, relative to a deep basin area, based on eco-biozones, ^{14}C -dated ages, event stratigraphy, lithostratigraphy, petrophysical properties and paleomagnetic measurements. Furthermore, the reliability of the reflectance parameter 550 nm% is evaluated as an independent correlation tool for tuning marine records.

2. Geological setting

Core C08 was collected in the Sentinelle Valley of the Sardinia Channel, 55 km from the mouth of the Bizerte Canyon, equidistant

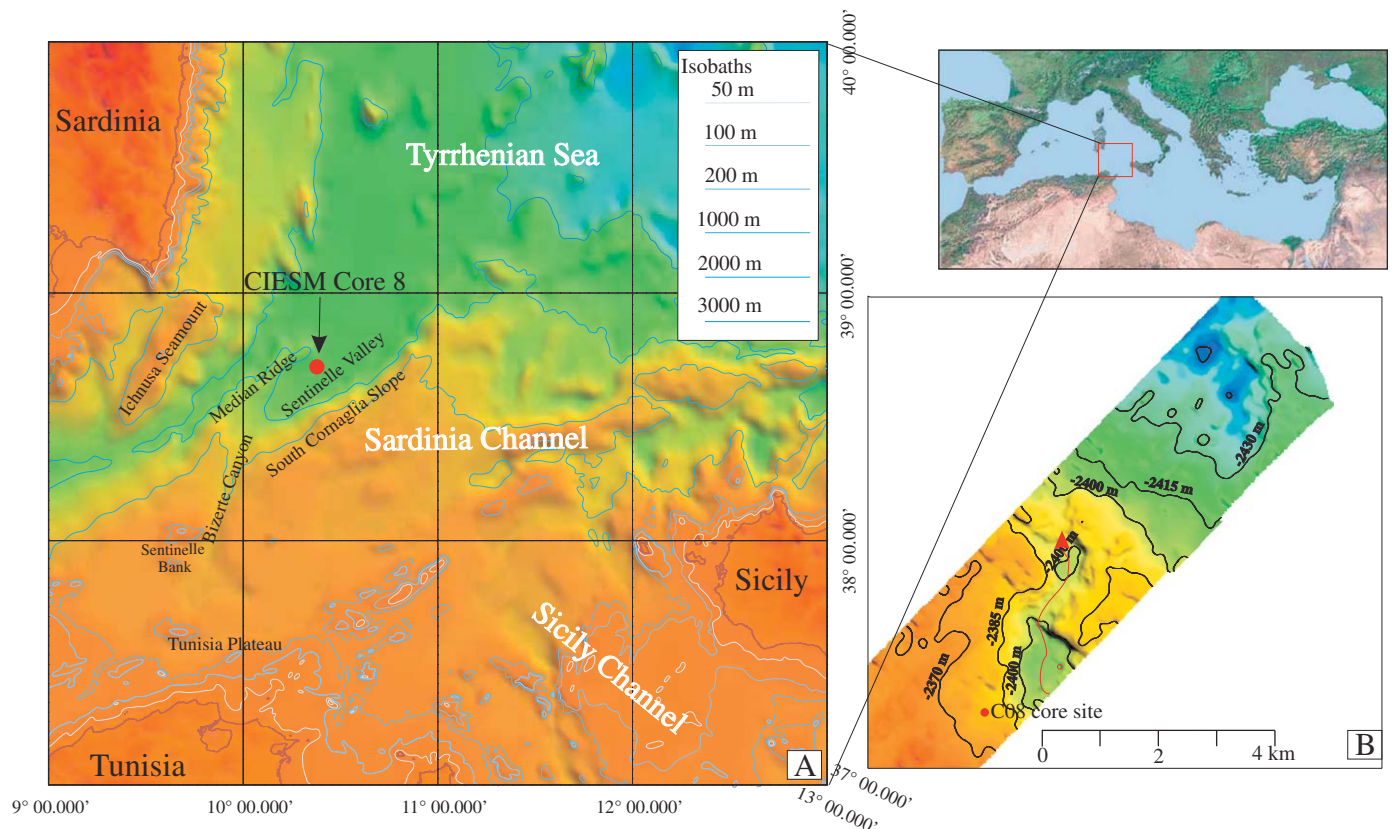


Fig. 1. (A) Location map of CIESM core C08. Bathymetry from GEBCO (1997); (B) bathymetric detail of core site, close to a channel South–North oriented (red arrow).

from Sicily, Sardinia and Tunisia (Fig. 1), during the cruise CIEM Sub2 onboard the R/V *Urania* in December 2005 (38°38.5364'N, 10°21.5576'E—2370 m water depth). In this area a 400-km-long submerged sector of the Apennine–Maghrebic branch of the Alpine orogen separates the Tyrrhenian (Plio–Pleistocene in age) and the Algero Provençal (Miocene in age) oceanic basins. This sector of the chain was not completely fragmented during the opening of the basins (Masclé et al., 2004). Due to the relatively minor post-orogenic extension and the good preservation of morpho-structural features, the Sardinia Channel is an important area for the reconstruction of the geodynamic evolution of the Western Mediterranean sector and was recently investigated through submersible surveys (Masclé et al., 2001a, 2004). The triangular-shaped valley is bounded by a NE–SW-oriented Median Ridge on its northwestern side and by the South Cornaglia slope to the southeast. The southwestern sector of the Sentinelle Valley receives the sedimentary contribution from the Bizerte Canyon, which cuts the Tunisian Plateau and the south margin of the Sentinelle Bank (Masclé et al., 2001b). The canyon head appears disconnected from the Tunisian shelf margin and extends over an area of about 1000 km² at an average depth of about 500 m (Fig. 1). It represents a particular type of canyons since it is not fed by an emerged areas or by a fluvio-deltaic systems (Reading and Richards, 1994; Prins et al., 2000; Kenyon et al., 2002;), but it drains a wide submarine plateau.

3. Material and methods

The gravity corer entered the uppermost portion of a sedimentary sequence made up with lateral continuous parallel and thin reflectors (Sartori et al., 2001), possibly related to hemipelagic and turbiditic deposition. It recovered about 5.40 m of hemipelagic mud interlayered with three fine-to-medium sand turbidite layers of increasing thickness towards the top of the core (Fig. 2).

3.1. Physical property measurements

The physical properties of the core were measured at 1-cm steps in a fully automated GEOTEK Multi-Sensor Core Logger (MSCL), in the petrophysical laboratories of IAMC in Naples (Italy). The MSCL system includes a Bartington MS2E Point sensor, to measure the low-field magnetic susceptibility (MS) with a spatial resolution of 0.4 cm and a Minolta Spectrophotometer CM 2002 that records at 0.8-cm steps, the percentage of reflected energy (RSC) at 31 wavelengths in 10-nm steps, over the visible spectrum (from 400 to 700 nm). MS and RSC measurements were taken on the archive half, ~1 h after the core had been split. The split core was covered with cling film to protect the glass cover of the Minolta aperture while measuring. Both measurements, log plotted, were visually compared to detect similar trends and

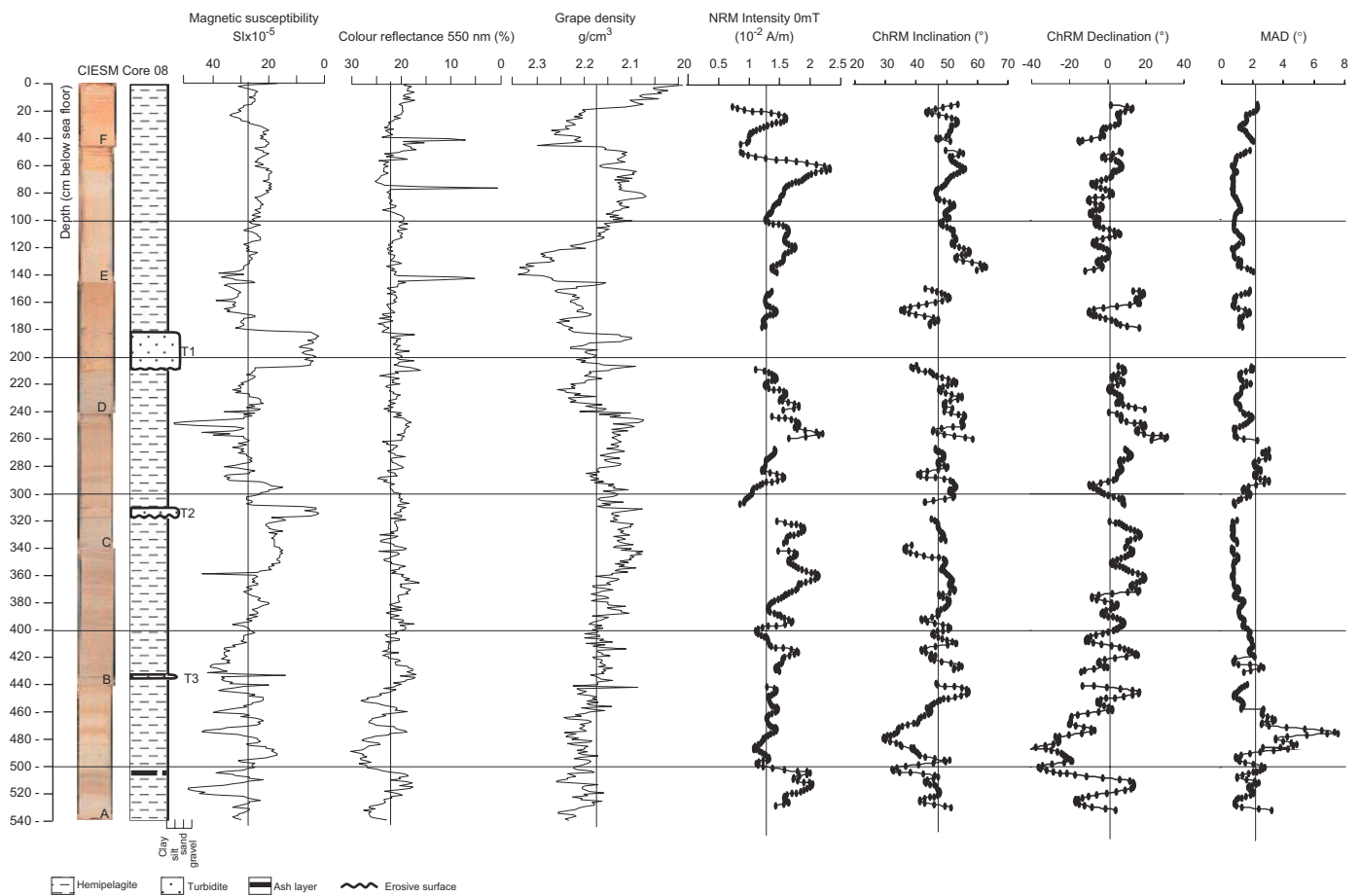


Fig. 2. Core CIEM 08: photography, lithologic log, petrophysical properties curves (magnetic susceptibility, reflectance 550 nm%, Grape density), paleomagnetic measurements curves (NRM intensity, ChRM inclination, ChRM declination, MAD) plotted against depth (cm below sea floor). In the paleomagnetic curves each dot represents a single measurement taken at 1-cm spacing. NRM: natural remanent magnetization; ChRM: characteristic remanent magnetization determined by principal component analysis on the demagnetization data; MAD: maximum angular deviation. The piston core was not azimuthally oriented, but a fiducial mark ensured the reciprocal orientation of each section from which u-channels were collected. The declination of each u-channel was rotated to bring the average value at 0°.

tentatively group the data according to their physical properties and corresponding stratigraphy (Wolf-Welling et al., 2001).

3.2. Paleomagnetic analysis

For the paleomagnetic study, 1-m-long u-channel specimens were sampled from archive halves of the CIESM 08 core. Only the turbiditic sandy interval at 182–208 cm depth was not suitable for u-channel sampling due to its coarse-grained and unconsolidated texture. The u-channels, sampled from the archive sections of the core, were measured in a magnetically shielded room at the paleomagnetic laboratory at the Istituto Nazionale di Geofisica e Vulcanologia in Rome, using an automated pass through a 2-G Enterprises DC SQUID cryogenic magnetometer system. For each u-channel the natural remanent magnetization (NRM) was measured at 1-cm steps. It is emphasized, however, that, due to the intrinsic response functions of the SQUID sensors, remanence measurements may be considered truly independent only every ca. 5 cm. The NRM was progressively demagnetized by the alternating field (AF) in nine steps up to a maximum field peak of 100 mT, by translating the u-channel through a set of three perpendicular AF coils at a speed of 10 cm/s. The remanence was measured at the same 1-cm spacing after each demagnetization step. Demagnetization data from u-channels were analysed on orthogonal vector projections and the paleomagnetic data obtained generally provided straightforward demagnetization diagrams, indicating that the sediments carry an almost single-component NRM. In fact, during the AF demagnetization a complete removal of any coring overprint and/or laboratory-induced remanences was achieved at low AF peaks (10 mT), and the characteristic remanent magnetization (ChRMs) of the sediments was clearly identified and determined by principal component analysis (Kirschvink, 1980). For each u-channel the uppermost and lowermost few cm were disregarded for the paleomagnetic analysis, to avoid any likely deflection of the remanence direction due to disturbances that may have been introduced during sampling. As stated before, no paleomagnetic data were collected for the coarse-grained level at 182–208 cm depth, and the NRM demagnetization diagrams did not allow a clear identification of a ChRM at 137–151 cm and 309–317 cm depth intervals.

3.3. Planktonic assemblage analysis

The analysis of planktonic foraminifera was conducted on 216 samples. Sampling spacing was 2 cm from the top of the core down to the base. Each wet sample of about 20 g was dried at 50 °C and washed over sieves with mesh-width size of 63 µm. Quantitative planktonic analyses were carried out on the fraction > 125-µm. The adopted taxonomic units were those reported by Jorissen et al. (1993) and Capotondi et al. (1999). According to these authors, we introduced some supraspecific categories (which remain unchanged even under bad preservation conditions), reducing the number of species actually occurring in the planktonic foraminiferal assemblages.

3.4. ¹⁴C Radiocarbon calibrations

About 10 mg of *Globigerina bulloides* and *Globorotalia inflata* were picked from three samples in the first 2 m beneath the sea floor (at the core top, at 0.44 and 1.43 mbsf) and were AMS radiocarbon dated at the Centre for Isotopic Research on Cultural and Environmental Heritage (CIRCE) radiocarbon laboratory, Caserta, (Italy). The CIRCE Accelerator Mass Spectrometry (AMS) system, based on the 3MV 9SDH-2 Pelletron accelerator, provides

a mean overall precision of 0.63% (Passariello et al., 2007). All radiocarbon dates were calibrated using the CALIB 5.0 Program and a mean ΔR value of 48 ± 21 yr (calculated among six of the Tyrrhenian Sea, from the marine data base of Stuiver and Reimer, 1993). The AMS RC age at 1.430 mbsf ($21,590 \pm 120$ a), close to the lower limit of the calibration curves, was not used for the age model.

4. Results

4.1. Lithostratigraphy and petrophysical properties

The sediment consists for the 95% of hemipelagic mud, ranging in colour from reddish and ochre to light, olive and dark grey; the remaining 5% are turbiditic sand layers (Fig. 2).

The uppermost 0.50 m consists of a reddish mud pervasively oxidized, then about 0.11 m of alternating dark grey and ochre laminated mud, and further below, 0.05 m of fine laminated ochre mud. From about 0.66 m down to 2.40 m olive grey mud occurs with rare dark patches, probably due to bioturbation, while from 2.40 m to the bottom of the core an alternation of several mud intervals occur, whose thickness range from cm to dm, showing different shades from light grey to dark grey. Three turbidite sand beds are interlayered in the mud sequence and occur from 1.82 to 2.08 m (T1), 3.10 to 3.17 m (T2) and 4.33 to 4.34 m (T3). They constitute 5% of the whole stratigraphic thickness of the core and are all characterized by low values of magnetic susceptibility. The turbidite layer T1 is marked by a sharp erosive contact and consists of a thin layer of oxidized sand, and then of a massive fine to medium sand with a high percentage of shell fragments; the upper boundary is sharp and the grain-size populations between fine sand and clay, which usually pertains to “b, c, d, e” divisions of the classical Bouma sequence (Bouma, 1962), are missing, as evidenced by the abrupt decrease of MS and Grape density values, which are a function of grain size and lithology. A sharp contact marks the onset of the turbidite layer T2, which contains a thin layer of well-sorted dark fine sand passing to a massive layer of well-sorted bioclastic fine sand; also in this case the upper boundary is sharp and the passage from massive and structureless sand to the hemipelagic mud is abrupt. Turbidite layer T3 has well-defined sharp boundaries and starts at the base with a thin layer of dark sand passing to light grey bioclastic sand. The thickness of the turbidites increases upward, but no sand layers occur in the uppermost 0.18 m of the core. A discrete fine ash layer, dark stained and characterized by diffuse boundaries occurs at 5.08 m and is marked by a MS peak value of $37 \text{ SI} \times 10^{-5}$. This tephra layer consists mainly of white pumice, dark green to yellowish glass shards, and few dark scoria; lithic elements are scarce (S. Tamburrino, pers. comm. 2007).

The lithologic features of the cored sediment are clearly detected by the petrophysical properties measured at a 1-cm steps: the volume magnetic susceptibility (MS) traces even thin tephra layers (Iorio et al., 2004), the GRAPE density is a compelling proxy for lithology and grain size (Wolf-Welling et al., 2001), and the reflectance at 550 nm wavelength provides a quantitative evaluation of variations in sediment colour and can serve as a powerful correlation tool between long-distance core sites (Peterson et al., 2000). For instance, the meter composite depth of ODP-Sites records (ODP-Leg 154, Curry et al., 1995) is composed on the variation in natural gamma rays, reflectance and magnetic susceptibility parameters, to identify sedimentary patterns and to calibrate marine records to the standard variation of astronomical parameters (Lourens et al., 1998; Palike et al., 2006).

The three turbidites are well evidenced by low MS values (T1 and T2 measuring less than $5 \text{ SI} \times 10^{-5}$, T3 of $12 \text{ SI} \times 10^{-5}$) and by GRAPE density value (close to 2.1 g/cm^3), but are not highlighted by RSC. The RSC parameter traces well the changes in shade colour throughout the core, and in particular it points out those occurring at the core top (due to the pervasive seabed sediment oxidation) and in the deepest 1.4 m (Fig. 2). Along this latter interval the wide oscillations in the RSC parameter, ranging between 15% and 30%, correspond to analogous oscillations in MS values.

4.2. Paleomagnetism

The main paleomagnetic results are plotted in Fig. 2, which shows the stratigraphic trend of the NRM intensity, the ChRM inclination and declination and the maximum angular deviation (MAD). The NRM is weak and unstable in the topmost 0.15 m of the core and will not be discussed in the following. The data from below 0.15 m show that NRM intensity is relatively high and characterized by a limited variation, with values oscillating between 0.6 and 2.3 (10^{-2} A/m). The ChRM inclination oscillates from 30° to 60° , with an average value of 48° that is about 10° lower than the expected value (58°) at the latitude of the coring site. Such a kind of shallow bias, or inclination error, has been found in laboratory redeposition experiments and in some modern natural sediments. The sedimentary inclination shallowing is a well-known process linked to the deposition of magnetic particles and subsequent sediment compaction (see Tauxe and Kent, 1984, 2004; Arason and Levi, 1990; Deamer and Kodama 1990; Tan et al., 2003; Tan and Kodama, 2003). The piston core was not azimuthally oriented, but a fiducial mark ensured the reciprocal orientation of each section from which u-channels were collected. The ChRM declination of each u-channel was rotated to bring the core average at 0° . Under this transformation the ChRM declination oscillates between -30° and $+30^\circ$, which is in the range of the expected geomagnetic secular variation. The principal component analysis of the demagnetization data shows a MAD always well below 3.3° along the core, which indicates a well-defined paleomagnetic direction, except a positive peak, up to a maximum of 7.5° , measured in the 0.47–0.48 m interval. This interval corresponds to the largest oscillations in the ChRM inclination and declination values, suggesting that some uncompensated lithological factor affects the paleomagnetic signal in that stratigraphic interval.

4.3. Quantitative distribution of planktonic foraminifera

A number of 13 species or groups of species were distinguished: *Globigerina bulloides* (including extremely rare specimens of *G. falconensis*); *Globigerinoides quadrilobatus* (including *G. trilobus* and very subordinate *G. sacculifer*); *Globigerinoides ruber* (including white and pink varieties, the latter extremely rare), *Globigerinoides elongatus* (very rare) and *Globigerinoides gomitolus* (very rare); *Globorotalia truncatulinoides* sl. right (very rare) and left coiling; *Globorotalia inflata* left coiling; *Globorotalia scitula* right and left coiling; *Globigerinoides tenellus* (rare); *Neogloboquadrina pachyderma* right and left coiling (extremely rare); *Globigerinita glutinata*; *Orbulina universa*; *Turborotalita quinqueloba*; *Globigerinatella siphoniphera* (rare) including *G. calida* (very rare); *Globoturborotalita rubescens* (rare).

The planktonic foraminifera, characterized by modern assemblages, are abundant and well-preserved, and the percentages of foraminiferal fragments are very low and do not alter the composition of the planktonic assemblage.

The long-term trend in planktonic foraminifera reveals that the faunal composition of the studied interval does not show drastic changes in the abundance patterns (Fig. 3). In particular, among the taxa that have a continuous distribution patterns, *G. bulloides*, *G. ruber*, *G. inflata* left coiled, *G. scitula* right coiled, *G. glutinata*, *N. pachyderma* right coiled and *T. quinqueloba* show long-term oscillation (trend) superimposed on short-term fluctuations possibly related to high-frequency climatic oscillations (Fig. 3).

Among the planktonic species having discontinuous distribution, *G. quadrilobatus*, *G. truncatulinoides* left coiled, *G. tenellus*, only occasionally reach significant percentages (Fig. 3).

5. Discussion

5.1. Planktonic foraminiferal eco-biozonation

Significant changes in the quantitative distribution of the planktonic foraminifera species allowed several authors (Asioli et al., 1999, 2001; Capotondi et al., 1999; Casford et al., 2002; Principato et al., 2003; Sprovieri et al., 2003; Ducassou et al., 2007) to define eco-biozones useful for fine-scale subdividing of the stratigraphic record. The eco-biozone boundaries are characterized by the temporary appearance or disappearance and/or evident abundance peaks of different taxa. In the present work, we refer the stratigraphic record to a slightly modified eco-biostratigraphic classification by Sprovieri et al. (2003). At present, the eco-biostratigraphic classification of Sprovieri et al. (2003) proposes nine eco-biozones over the last 23 kyr. Here, we propose to mark the base of eco-biozone nine with the strong increase of *G. inflata*, occurring in the Mediterranean area at about 30 ka (Ducassou et al., 2007; Geraga et al., 2005), and to extend eco-biozone 10 back to ~80 kyr. Actually, using the quantitative distribution pattern of the most abundant planktonic foraminifera species counted throughout C08, we identified 10 evident eco-biozones from top to bottom (Fig. 3).

The uppermost part of the studied record attributed to eco-biozone 1, which extends down to 0.08 m, is characterized by a decrease in abundance of *G. quadrilobatus* and the end of *G. truncatulinoides* right coiled. This attribution is also supported by a ^{14}C -AMS calibration, which dates 2.18 ka cal. BP (Fig. 3; Table 1).

Eco-biozone 2 is defined by the concomitant abundance of *G. quadrilobatus* and *G. truncatulinoides* left and right coiled and low abundance values of *N. pachyderma* right coiled in the lower part. A strong increase of *G. truncatulinoides* left coiled marks the base of the eco-biozone (Fig. 3).

The short interval represented by eco-biozone 3, whose base is at 0.31 m, is marked by the end of the micropaleontological signature of sapropel S1 and is characterized by low abundances of *T. quinqueloba*, *G. quadrilobatus*, and *G. truncatulinoides* left coiled.

Eco-biozone 4 corresponds to the time interval of sapropel S1 deposition, although no lithological evidence was found except for colour shades (Fig. 2). *G. ruber* oscillations allowed a reliable identification of the faunal signature of the climatic events associated with the deposition of sapropel S1 (Fig. 3). In particular, two distinct peaks in *G. ruber* mark the two short-term warm oscillations (S1a and S1b, Sprovieri et al., 2003), separated by a cold phase (Fig. 3). A ^{14}C -AMS datum at 0.44 mbsf (within the cold phase) gives an age of 8.79 ka cal. BP (Table 1), coincident with an increase in abundance of *G. tenellus* and *G. quadrilobatus* (Sprovieri et al., 2003).

Eco-biozone 5 is defined by the concomitant occurrence of *G. ruber* and *G. inflata*, by a distinct peak of *G. truncatulinoides* left

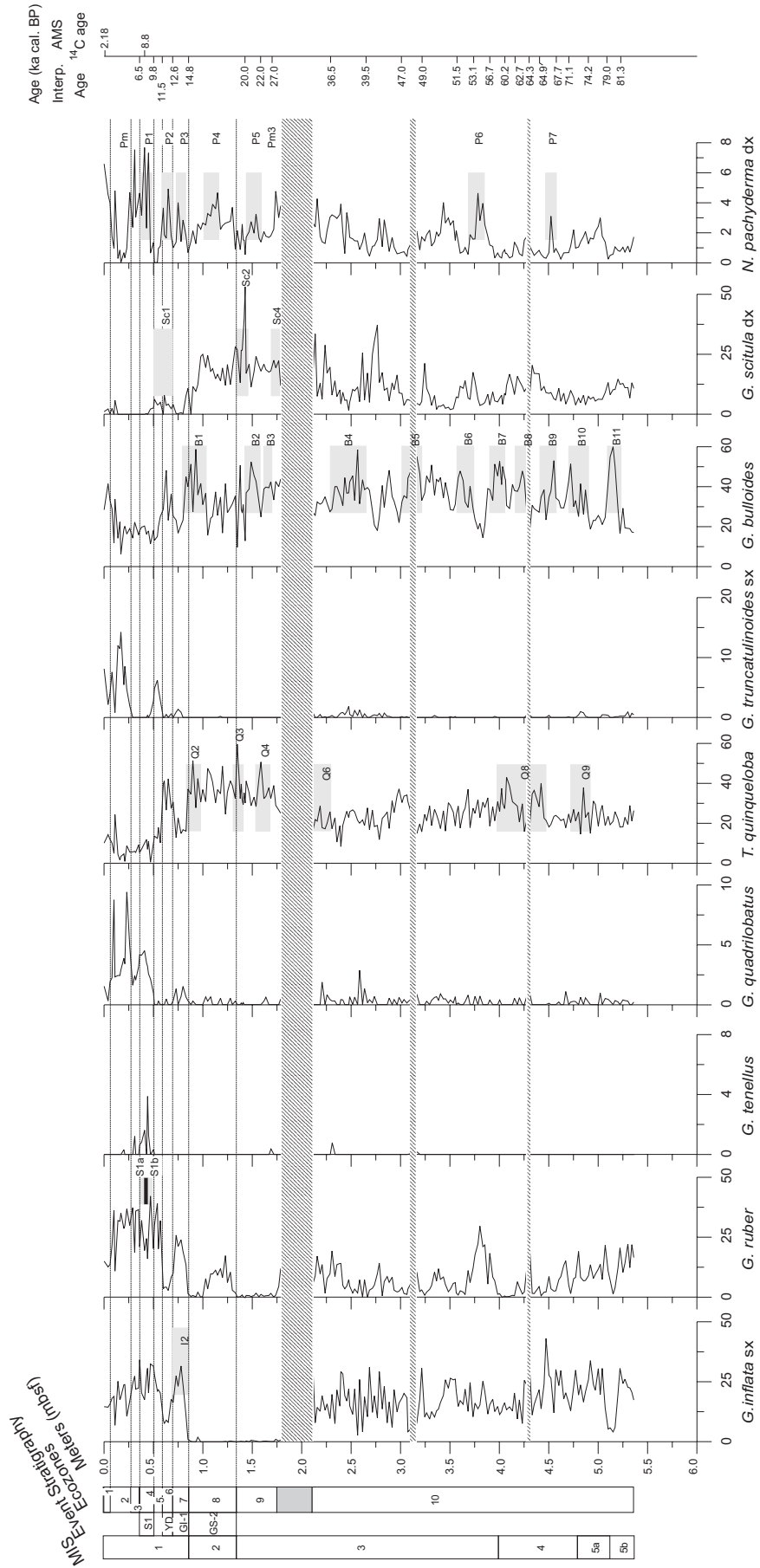


Table 1
Tie points used for age–depth profile of core C08.

| Events | mbsf | Age (ka cal. BP) | References |
|----------------------|-------|---------------------|---|
| AMS ¹⁴ C– | 0 | 2.18 | This work |
| Top S1 | 0.360 | 6.5 | Casford et al. (2002) (Aegean Sea) |
| AMS ¹⁴ C– | 0.440 | 8.8 | This work |
| Base S1 | 0.470 | 9.8 | Casford et al. (2002) (Aegean Sea) |
| Top YD | 0.570 | 11.5 | Asioli et al. (2001) (Adriatic Sea) |
| Base YD | 0.700 | 12.6 | Asioli et al. (2001) (Adriatic Sea) |
| Base GI-1 | 0.850 | 14.8 | Asioli et al. (2001) (Adriatic Sea) |
| Base GS-2 | 1.350 | 20 | Andersen et al. (2006) (Greenland Ice core) |
| AMS ¹⁴ C– | 1.430 | 25.1 | This work (not used in the age model) |
| Base B2 | 1.540 | 22 | Pérez-Folgado et al. (2003) (Alboran Sea) |
| Top B3 | 1.620 | 25.3 | Pérez-Folgado et al. (2004) (Alboran Sea) |
| Base B3 | 1.720 | 27 | Pérez-Folgado et al. (2003) (Alboran Sea) |
| Top B4 | 2.360 | 36.50 | Pérez-Folgado et al. (2004) (Alboran Sea) |
| Base B4 | 2.690 | 39.50 | Pérez-Folgado et al. (2004) (Alboran Sea) |
| Top B5 | 3.040 | 47.00 | Pérez-Folgado et al. (2004) (Alboran Sea) |
| Base B5 | 3.200 | 49.00 | Pérez-Folgado et al. (2004) (Alboran Sea) |
| Top B6 | 3.570 | 51.50 | Pérez-Folgado et al. (2004) (Alboran Sea) |
| Base B6 | 3.740 | 53.10 | Pérez-Folgado et al. (2004) (Alboran Sea) |
| Top B7 | 3.875 | 56.70 | Pérez-Folgado et al. (2004) (Alboran Sea) |
| Base B7 | 4.075 | 60.20 | Pérez-Folgado et al. (2004) (Alboran Sea) |
| Top B8 | 4.125 | 62.70 | Pérez-Folgado et al. (2004) (Alboran Sea) |
| Base B8 | 4.275 | 64.30 | Pérez-Folgado et al. (2004) (Alboran Sea) |
| Top B9 | 4.430 | 64.90 | Pérez-Folgado et al. (2004) (Alboran Sea) |
| Base B9 | 4.610 | 67.70 | Pérez-Folgado et al. (2004) (Alboran Sea) |
| Top B10 | 4.680 | 71.10 | Pérez-Folgado et al. (2004) (Alboran Sea) |
| Base B10 | 4.910 | 74.20 | Pérez-Folgado et al. (2004) (Alboran Sea) |
| Top B11 | 5.080 | 79.00 | Pérez-Folgado et al. (2004) (Alboran Sea) |
| Base B11 | 5.210 | 81.30 | Pérez-Folgado et al. (2004) (Alboran Sea) |

The *Globigerina bulloides* eco-bioevents B3–B11 follow Pérez-Folgado et al. (2003, 2004).

coiled, and by the absence of *N. pachyderma* right coiled and very low amounts of *T. quinqueloba*.

The eco-biozone 6 is marked by the absence of *G. ruber* and *G. inflata* left coiled, by distinct peaks of *T. quinqueloba* and *N. pachyderma* right coiled. This eco-biozone corresponds to the Younger Dryas event, according to Sprovieri et al. (2003).

Eco-biozone 7 is defined by the increase in the abundance of *G. ruber* and *G. inflata*, by the absence of *T. quinqueloba*, and by a distinct peak of *G. quadrilobatus*, corresponding to the warmer (interstadial) GI-1.

According to Sprovieri et al. (2003) in eco-biozone 8 the persistent high abundance of cold species permit correlation of this interval with the GRIP GS-2 period. In particular this eco-biozone is dominated by *T. quinqueloba*, *N. pachyderma* right coiled, *G. scitula*, and by absence of *G. inflata* left coiled and rare *G. ruber*. The base of this eco-biozone approximates to the base of MIS 2 (Pérez-Folgado et al., 2003) (Fig. 3).

Eco-biozone 9 is characterized by the concomitant absence of *G. inflata* left coiled and *G. ruber*, by low abundance of *N. pachyderma* right coiled, and by high abundance of *T. quinqueloba* and *G. scitula* right coiled.

Eco-biozone 10 is clearly marked by the progressive downward increase in abundance of *G. inflata* left coiled and *G. ruber* and the progressive decrease of *G. scitula* right coiled, *T. quinqueloba*, *N. pachyderma* right coiled and *N. dutertrei* right coiled (Fig. 3). No distinctive or drastic events in the planktonic faunal patterns are visible towards the base of the studied record but only short-term oscillation in *G. bulloides* (B3–B11 eco-bioevents; the adopted

sampling resolution unfortunately did not allow the recognition of the *G. bulloides* B8 eco-bioevent), *G. inflata* left coiled (I3–I5 eco-bioevents), *T. quinqueloba* (Q4–Q9 eco-bioevents) and *N. pachyderma* right coiled (P5–P7 eco-bioevents), clearly associated to the millennial climatic oscillations occurring in the last 80 kyr (Pérez-Folgado et al., 2004). According to Pérez-Folgado et al. (2004) *G. bulloides* eco-bioevents B7 and B10 are placed at the MIS 4/MIS 3 and MIS4/MIS 5a transitions, respectively. Finally, also according to Pérez-Folgado et al. (2004), the lowermost part of the studied record lies within the eco-bioevent B11 and within the uppermost part of MIS 5b (Fig. 3).

5.2. Age model

The identified foraminiferal marker events, regarded to reflect major changes in oceanographic conditions and already recognized in the central and Western Mediterranean (Jorissen et al., 1993; Capotondi et al., 1999; Asioli et al., 2001; Scaffi et al., 2004; Sprovieri et al., 2003; Pérez-Folgado et al., 2004; Geraga et al., 2005), were used, together with two ¹⁴C-AMS dates (Table 1), to constrain the age of core CIESM C08 and strengthen the correlations between the various Mediterranean sites. In particular, we used the age model proposed by Pérez-Folgado et al. (2003, 2004) for the Alboran Sea to recognize the top and base of the eco-bioevents recorded in the core C08, the age model proposed by Asioli et al. (2001) for the Adriatic Sea, to identify the Younger Dryas and the base of the Greenland isotope interstadial 1 (GI-1), and the age model of Andersen et al. (2006) for the NGRIP record to distinguish the Greenland isotope stadial 2 (GS-2) (Table 1).

During the recovery of the core, a small amount of the core top may have been lost, which is seen by the ¹⁴C-AMS dating of 2.18 ka cal. BP at the top of the core and by comparing the planktonic foraminiferal contents of the studied record with those reported by Sprovieri et al. (2003) for ODP-Site 963 (Sicily Channel). This seems to confirm that the sedimentation of the last 2000 years is not preserved in CIESM C08 core.

The turbidite layers T1, T2 and T3 have been taken into account to construct the age model curve and to estimate sedimentation rates. A second-order polynomial is needed to describe the age–depth relationship for the studied record, indicating an average sedimentation rate of ~7 cm/kyr from the base to the top and four main excursions (Fig. 4).

In order to confirm the reliability of the proposed age model, a three-step validation process was performed. First, the visual comparison, in time domain, between *G. bulloides* distribution pattern of Pérez-Folgado et al. (2004) for the Alboran Sea and the patterns in core CIESM C08 (Fig. 4), confirmed the tuning accuracy.

The second step consisted of the comparison of colour reflectance record at 550 nm (%) of core CIESM C08 with the record of the ODP-Site 964 (Fig. 5), drilled in the Ionian Sea at 3650 mbsl and astronomically calibrated (Lourens, 2004). Using the proposed age–depth profile (Fig. 4), the colour reflectance record of the studied core was plotted against time by a cubic spline interpolation method. This comparison (Fig. 5) shows that the large-scale reflectance fluctuations in core CIESM C08 not only have a similar pattern to those reported in the Ionian Sea record but also encompass absolute values in the same range (± 10 nm).

Fig. 3. Relative abundance of selected planktonic foraminifera from core CIESM C08 plotted vs depth (m bsf). Eco-biozones 1–10 are identified, according to Sprovieri et al. (2003), slightly modified. Grey bands show the selected eco-bioevents proposed by Pérez-Folgado et al. (2003, 2004). Event stratigraphy according to GRIP. MIS and age scale according to Pérez-Folgado et al. (2003, 2004). Associated with the *G. ruber* curve, two grey bands interbedded with the black one correspond to the position of sapropel 1 equivalent with S1a and S1b. The banded areas indicate the position of the turbidite layers.

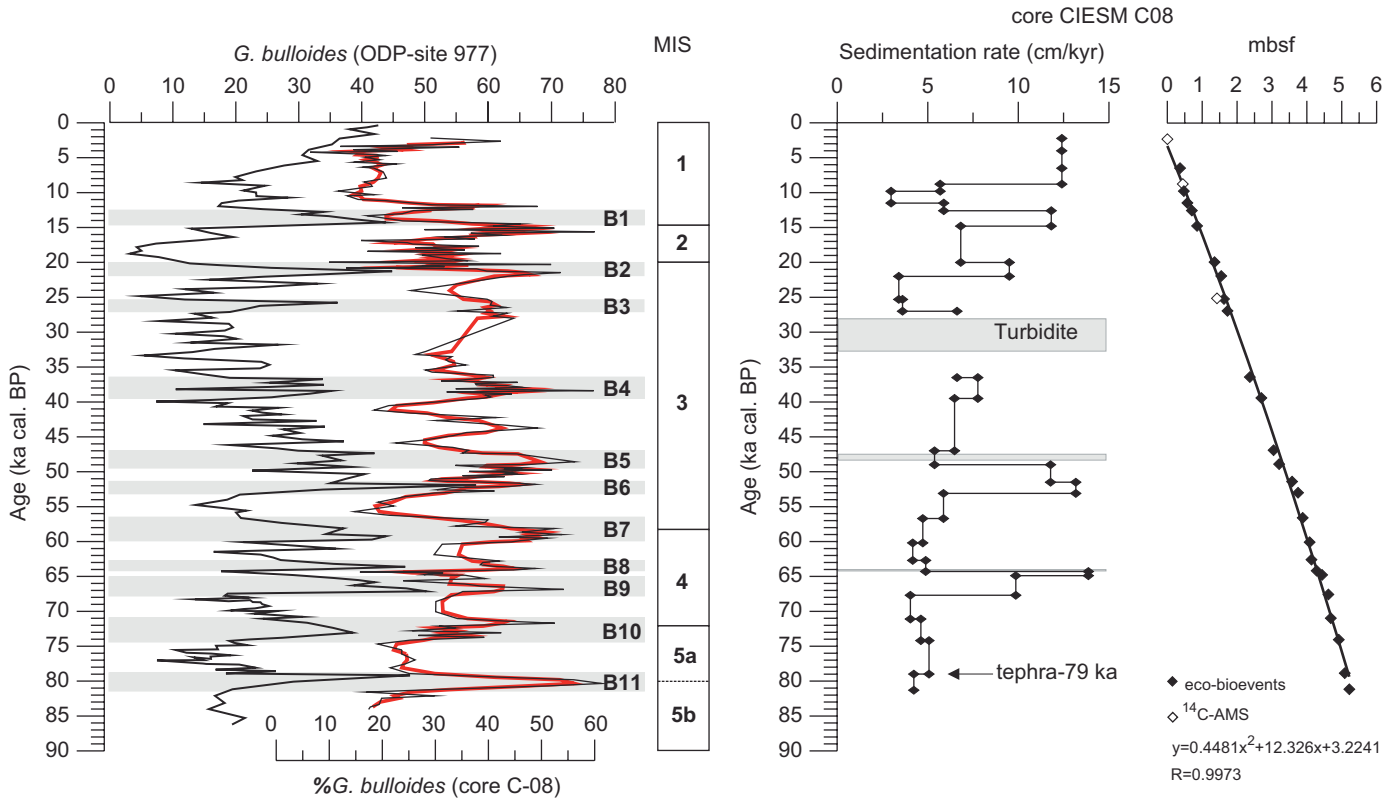


Fig. 4. From left to right: comparison in time domain between the distribution pattern of *G. bulloides* from ODP-Site 977 (Perez-Folgado et al., 2004) and the studied core CIESM C08 (the red curve represents a 3-point average). The grey bands and the labels B1 to B11 are from Perez-Folgado et al., (2004). Age–depth profile and sedimentation rates of core CIESM C08. The adopted tie-points by eco-bioevents and by ¹⁴C-AMS data are shown respectively with black boxes and white boxes.

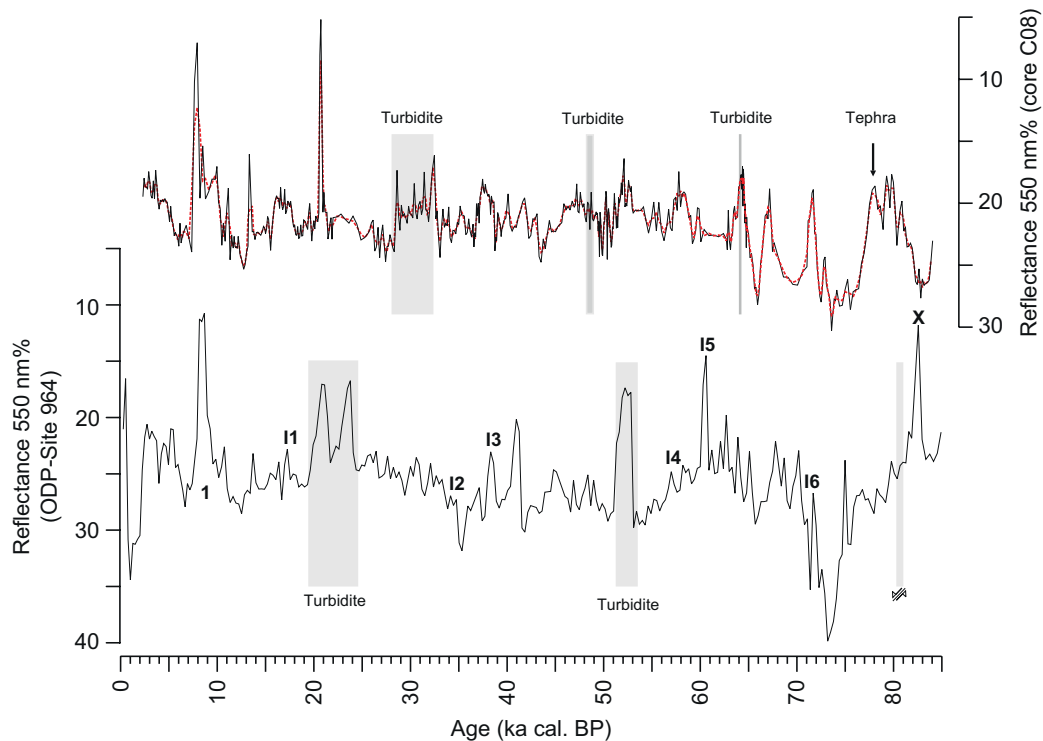


Fig. 5. Comparison in time domain of colour reflectance data of core CIESM C08 (black curve, with 3-point average, red dotted curve) with reflectance data after Lourens (2004) for ODP-Site 964 (thin black curve) in the Ionian Sea. The numbers I1–I6 indicate tephra layers in ODP-Site 964, and 1 and X indicate the position of the sapropel 1 and X, respectively.

Lourens (2004) used the reflectance parameter to detect sapropel and tephra layers in the Ionian Sea (Mediterranean area), which in turn, are tuned to the insolation curve of Laskar et al. (2004). According to Hilgen et al. (2003 and references therein), the Neogene marine successions (on land and in ODP-sites) in the Mediterranean area are often characterized by the cyclic recurrence of sapropels layers and sedimentary patterns, clearly forced by variation in astronomical parameters (Hilgen, 1991a,b; Hilgen et al., 1999, 2003; Hilgen and Krijgsman, 1999; Lourens et al., 1996a,b, 1998 and references therein). Therefore it is not surprising that the cyclic patterns in the colour reflectance records relative to two adjacent deep environmental Mediterranean areas are similar. There is also a strong similarity between the colour reflectance signature of the sapropel S1 equivalent, recorded in the studied core, with the sapropel S1 colour reflectance signature in the Ionian basin. Nevertheless, some of the minimum peaks of the ODP-Site 964 reflectance record, related to the occurrence of tephra layers, are not present in the studied core. This is clearly due to the different spatial distribution of the tephra layers in the Mediterranean. On the whole, the good visual correlation obtained between the two records supports the validity of the age model based on the identified eco-bioevents and ¹⁴C-AMS calibrations.

The third control step consisted in the comparison of the *G. ruber* distribution with the $\delta^{18}\text{O}$ NGRIP ice core record. The ecological features of *G. ruber* associated with warm and oligotrophic surface waters have been established in several oceanographic settings (Hemleben et al., 1989; Pujol and Vergnaud-Grazzini, 1995; Watkins et al., 1996; Zaric et al., 2005). Moreover, several authors (Sprovieri, 1991; Sanvoisin et al., 1993; Sprovieri et al., 2003, 2006) have confirmed the utility of relative abundance fluctuations of *G. ruber* as recorders

of climatic variability and for age model proxies. The *G. ruber* and $\delta^{18}\text{O}$ NGRIP ice core records exhibit a remarkable agreement, with the identification of the Heinrich events (H1–H6) and of the Younger Dryas (YD) in the studied record, which further supports the reliability of our tuning (Fig. 6). The observed strong link between $\delta^{18}\text{O}$ of Greenland ice cores, a proxy for Greenland air temperature, and the thermal character of surface water masses of Mediterranean area has been previously established in several papers and is usually explained by teleconnective phenomena (Rohling et al., 1998; Cacho et al., 1999, 2000; Saffi et al., 2004; Combourieu Nebout et al., 2002; Moreno et al., 2002; Rohling et al., 2002).

The proposed age model also was adopted to plot paleomagnetic data against time (Fig. 7). We note that the time interval spanned by the core encompasses three known geomagnetic excursions (the Mono Lake, dated at 33 ± 1 ka; the Laschamp, dated at 41 ± 1 ka; the Norwegian-Greenland Sea, dated at 61 ± 2 ka; see Lund et al., 2006). Nevertheless in the paleomagnetic record of CIESM C08 core there is no clear marked oscillation that can be ascribed to any of such excursions. The lack of paleomagnetic evidence for geomagnetic excursions in this record may be due to a relatively low sedimentation rate (cf. 5.1, Fig. 4), which may have resulted in a prolonged time interval for the lock-in of the natural remanence of the sediments (Roberts and Winklhofer, 2004; Sagnotti et al., 2005), as well as response functions of the SQUID sensors in the magnetometer (i.e. Oda and Shibuya, 1996; Guyodo et al., 2002). Despite the suggested smoothing of the paleomagnetic signal, the well-defined paleomagnetic data of core CIESM-08 provide an original source of information to improve the confidence of geomagnetic paleosecular variation reconstructions in the Mediterranean for the last 83 kyr.

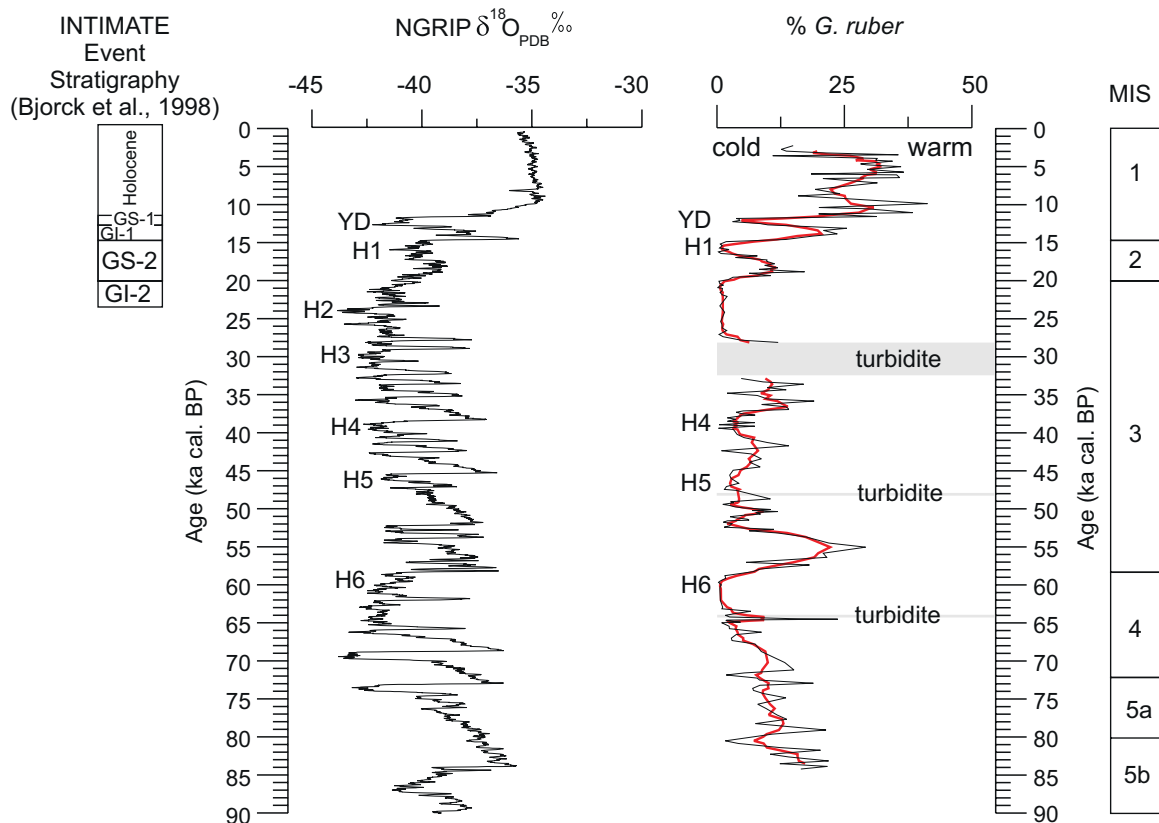


Fig. 6. Distribution pattern of *G. ruber* (thin black line) with 3-point average (red line) of core CIESM C08 plotted versus $\delta^{18}\text{O}$ NGRIP (NGRIP members, 2004) record, with 7-point average, in time domain. Labels H1 to H6 indicate the position of Heinrich events and the label YD the position of the Younger Dryas.

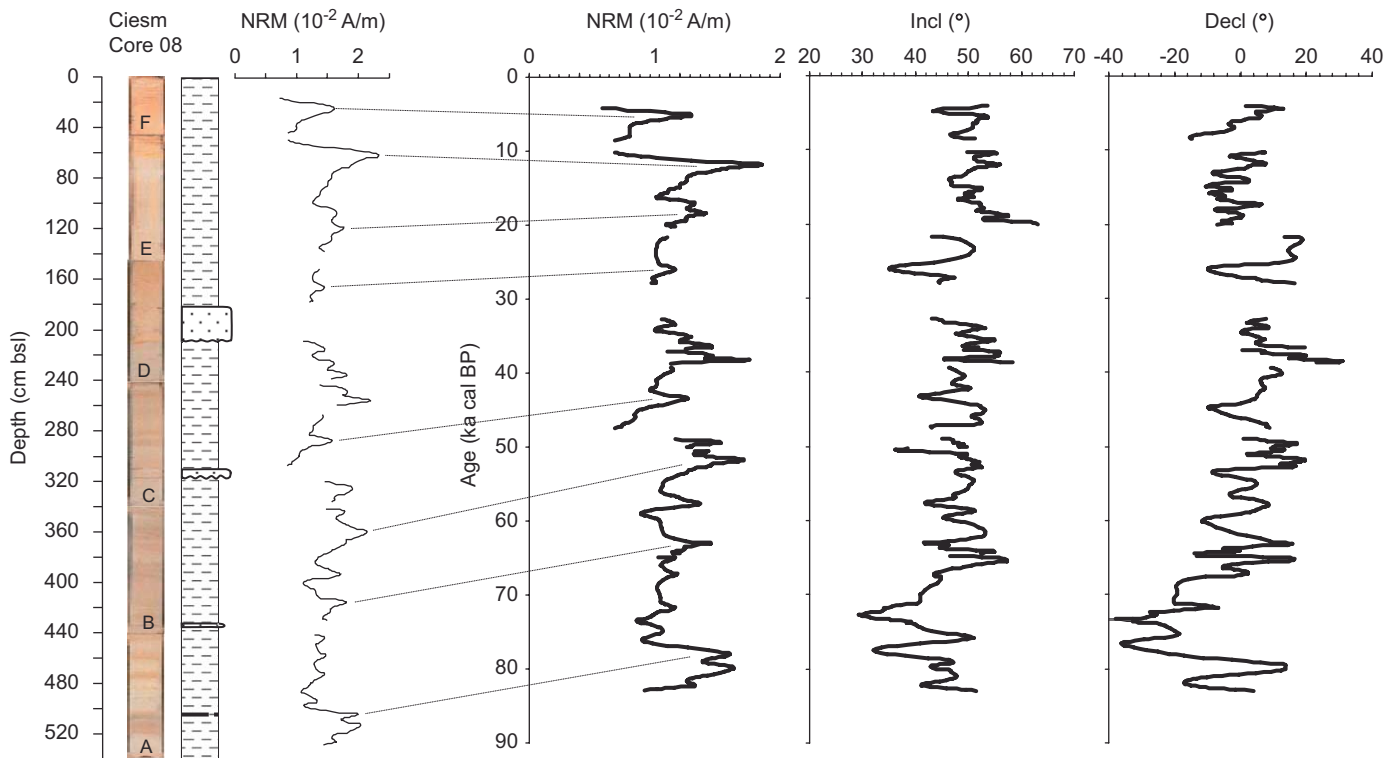


Fig. 7. Downcore plot of paleomagnetic data. The NRM intensity plotted versus stratigraphic depth is shown beside to the main paleomagnetic data (NRM, inclination and declination of the characteristic remanent magnetization) plotted versus age, according to the independently derived age model discussed in this study.

5.3. Provenance and ages of turbidite events

The size population of grains, the grain fabric, the high content in bioclasts (gastropod, bivalve and echinoderm debris) and the features of the surfaces bounding T1, T2 and T3 turbidites lead us to infer a distant source of transported material, since it seems to have been remobilized from areas of high productivity. Both the slope of the Median Ridge and the southern Cornaglia slope (Fig. 1) can be ruled out as possible source areas for these sand-rich bioclastic turbidites, since they are too deep, respectively 1300 and 1000 mbsl. Sartucya 6 diving survey (Masclé et al., 2001a) showed that the base of the southern slope of the Median Ridge (2270–1940 mbsl) is draped with mud, shaped by current bed-forms, while the upper slope (1990–1640 mbsl) is characterized by conglomerates and sandstone layers outcropping from the mud, then volcanic rocks. The lithology to the southern Cornaglia slope was described during the Sarcya 2 submersible diving (Masclé et al., 2001a) by the occurrence of pelagic mud at 2500–2250 mbsl, and cemented coarse material on the steep slopes (2250–2060 mbsl). Although several canyons are noted along the Southern Cornaglia slope (Brocard, 2001), they enter the Sentinelle Valley seaward to the core site and thus they possibly feed the deepest parts of the basin.

Thus, we must infer that the Bizerte Canyon acted as the main conduit to transport the bioclastic sand from high productivity areas on the Tunisian plateau (Fig. 1), inferring transport of more than 50 km before sedimenting. As highlighted by many authors (Walker, 1967; Normark et al., 1984; Reading and Richards, 1994) gentle gradient slopes or pre-existing slope conduits can drive very efficient density currents (Damuth and Flood, 1984; Richards et al., 1998) able to cover long distances quickly and to “segregate the original grain populations into distinct and relatively well-sorted facies types with distances” (Mutti et al., 1999). The beds occurring in C08 core, in particular T1 and T2, could correspond to the facies tract F7 in Mutti et al. (1999), composed predominantly

of medium to fine grained well-sorted sand. In fact in this model, which associates the horizontal grain-size partition of the deposit with the different degrees of flow efficiency, the F7 facies tract consists of medium to fine sand overlying a mm-thick traction carpet that accounts for the development of an erosion surface at the base. This model may explain why T1 and T2 turbidites lack parallel and ripple lamination and pelitic division and why a wide stratigraphic gap occurs at the T1 base (and likely at the T2 base).

The turbidite layers in CIESM core C08 are confined in the lower 4 m of the core and their thicknesses increase upward, peaking at T1 (Fig. 2) and pointing to a general regressive trend. Through the age model scheme of CIESM C08 core here proposed, it is possible to date T layers, respectively, at 28 ka cal. BP (T1), 48 ka cal. BP (T2) and 64 ka cal. BP (T3) (Fig. 5), thus during the MIS 4 and MIS 3. The emplacement of T1 event bed caused the removal of an undefined thickness of hemipelagic mud corresponding to a time span of about 4 kyr (Fig. 4).

Plotting their inferred age on sea-level curve relative to the last 100 kyr (Waelbroeck et al., 2002; Imbrie et al., 1984), T2 and T3 turbidite event beds appear to correlate with two relative sea-level low stands, and T1 with regressing sea level that led to the maximum low stand at ~20 kyr (Fig. 8). This observation seems to agree with the most accepted stratigraphic models of deep-sea deposition (Normark et al., 1998). Thus, the part of the basin fan intercepted by the CIESM core C08 was actively fed with bioclastic sand deposition during the relative sea-level minimum and increased its transport efficiency following the sea level lowering. Nevertheless the CIESM core C08 does not record any further sand deposition during the MIS 2 sea-level low stand. A rapid starvation in detritus supply occurred in this area beginning at 28 ka cal. BP and this sector of the fan fossilized below a drape of hemipelagic mud. It is reasonable to suppose that during this phase, this sector of the fan acted mainly as a bypass area. Thus, any possible sand flow would have been deposited basinward.

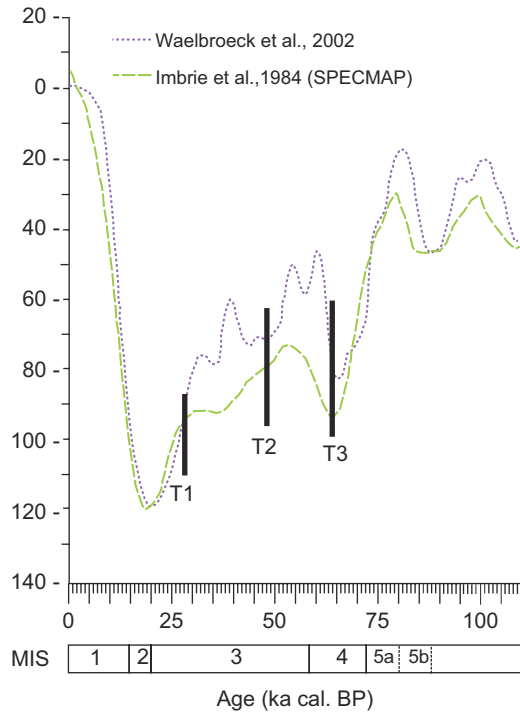


Fig. 8. The inferred age of turbidite sand beds is plotted relative to the sea level over the past 100 kyr (from Antonioli et al., 2004, modified). T2 and T3 turbidites occur during two relative low-stand phases of MIS 4 and 3, while the T1 turbidite falls during the last sea level lowering of MIS 3.

6. Conclusions

The multidisciplinary study of core C08, recovered from the deep sector of the Sardinia Channel, based on planktonic foraminiferal assemblages, petrophysical (MS, Grape density, 550 nm% reflectance) and paleomagnetic (NRM Intensity, ChRM Inclination, ChRM Declination) data, provides an integrated stratigraphic reference record for the Western Mediterranean Sea that spans back for about 83 kyr. The most important eco-bioevents widely used for large-scale correlation in the Western Mediterranean area provide a detailed correlation with the eco-stratigraphic reconstruction proposed by Perez-Folgado et al. (2003, 2004) for the Alboran Sea.

In particular, the relative abundance of selected climate-sensitive planktonic foraminiferal species have led us to identify several eco-bioevents in *G. bulloides* (B3–B11 eco-bioevents), *G. inflata* left coiled (I3–I5 eco-bioevents), *T. quinqueloba* (Q4–Q9 eco-bioevents) and *N. pachyderma* right coiled (P5–P7 eco-bioevents). According to Perez-Folgado et al. (2003, 2004), the documented short-term oscillations in the planktonic foraminiferal fauna are clearly associated with the stadial/interstadial excursions over the last 80 kyr, allowing the identification in core C08 of the S1, YD, GI-1 and GS-2 climatic events in the last 23 kyr. Furthermore, the comparison between the $\delta^{18}\text{O}$ NGRIP ice core record and *G. ruber* distribution in core C08 suggests that the Heinrich events (H1–H6) and the Younger Dryas (YD) are also recorded.

The eco-bioevents chronology combined with ^{14}C -AMS data were used to define a detailed age model that was compared by means of reflectance parameters to the astronomically tuned age model proposed for the Ionian Sea ODP-Site 964 (Lourens, 2004). The similarity between the two reflectance records plotted vs time validates the age model of the studied record, especially in the time intervals between 2–25 and 60–83 kyr. This methodology, if confirmed with further study, could prove a powerful tool for

reliably correlating marine records between comparable deep-sea settings.

The sector of the Sentinelle Valley intercepted by the CIESM core C08 has been sporadically fed by sand turbidite flows, likely driven along the Bizerte Canyon from the northern sector of the Tunisian Plateau, during relative sea-level minimum and sea-level fall of MIS 4 and 3. This sector of the basin was reached by three sand deposition events of increasing thickness between 64 and 28 kyr. After about 28 kyr this part of the fan was deactivated and fossilized beneath a carpet of hemipelagic mud at a sedimentation rate of about 7 cm/kyr.

The combined logging of sedimentological, petrophysical and paleomagnetic data of core CIESM C08, integrated with eco-biozone stratigraphy, could provide an important source of information to improve the confidence of correlations in the Mediterranean over the last 83 kyr. In this framework, future efforts will be focused on the comparison of the ChRM directions obtained for the core with the other available European geomagnetic paleosecular variation records, as well as on the reconstruction of a relative geomagnetic paleointensity curve, to establish a Mediterranean paleomagnetic reference record to be used as an original dating tool for coeval sequences of this region.

Acknowledgements

The authors gratefully acknowledge Lucas J. Lourens of the University of Utrecht for original reflectance data of Ionian cores and Carmine Lubritto of CIRCE Radiocarbon Laboratory, (Caserta, Italy) for ^{14}C -AMS dates. Sincere thanks are also due to Laura Giuliano, who involved some of us in CIESM SUB2 cruise. Captain Vincenzo Lubrano di Lavadera and the crew of R/V *Urania*, who sailed despite a very rough sea, are kindly acknowledged. Two anonymous reviewers and Patricia Scalfani are sincerely thanked for the comments and the English revision to the manuscript.

References

- Andersen, K.K., Svensson, A., Johnsen, S.J., Rasmussen, S.O., Bigler, M., Rothlisberger, R., Ruth, U., Siggaard-Andersen, M.L., Steffensen, J.P., Dahl-Jensen, D., Vinther, B.M., Clausen, H.B., 2006. The Greenland ice core chronology 2005, 15–42 ka. Part 1: Constructing the time scale. *Quaternary Science Reviews* 25, 3246–3257.
- Antonioli, F., Bard, E., Potter, E.K., Silenzi, S., Improta, S., 2004. 215-ka history of sea-level oscillations from marine and continental layers in Argentarola Cave speleothems (Italy). *Global and Planetary Change* 43 (1–2), 57–78.
- Arason, P., Levi, S., 1990. Models of inclination shallowing during sediment compaction. *Journal of Geophysical Research* 95, 4481–4499.
- Ariztegui, D., Asioli, A., Lowe, J.J., Trincardi, F., Vigliotti, L., Tamburini, F., Chondrogiani, C., Accorsi, C.A., Bandini Mazzanti, M., Mercuri, A.M., Van der Kaars, S., McKenzie, J.A., Oldfield, F., 2000. Palaeoclimate and the formation of sapropel S1: inferences from Late Quaternary lacustrine and marine sequences in the central Mediterranean region. *Palaeogeography, Palaeoclimatology, Palaeoecology* 158, 215–240.
- Asioli, A., Trincardi, F., Lowe, J.J., Oldfield, F., 1999. Short-term climate changes during the last Glacial–Holocene transition: comparison between Mediterranean and North Atlantic records. *Journal of Quaternary Science* 4, 3732–3781.
- Asioli, A., Trincardi, F., Lowe, J.J., Ariztegui, D., Langone, L., Oldfield, F., 2001. Sub-millennial scale climatic oscillations in the central Adriatic during the Lateglacial. *Paleoceanographic implications. Quaternary Science Review* 20, 1201–1221.
- Beaudouin, C., Dennielou, B., Melki, T., Guichard, F., Kallel, N., Berné, S., Huchon, A., 2004. The Late-Quaternary climatic signal recorded in a deep-sea turbiditic levee (Rhône Neofan, Gulf of Lions, NW Mediterranean): palynological constraints. *Sedimentary Geology* 172 (1–2), 85–97.
- Bouma, A.H., 1962. *Sedimentology of Some Flysch Deposits, a Graphic Approach to Facies Interpretation*. Elsevier, Amsterdam.
- Brocard, G., 2001. Le canal de Sardaigne au Néogène: analyse morphologique et structurale. Apports de la bathymétrie multifaisceaux et des plongées Sarcya et Sartucya. In: Mascle, G., Tricart, P. (Eds.), *Le Canal de Sardaigne: les plongées Cyana*, vol. 34. *Geologie Alpine, Mém. H.S.*, pp. 115–166.
- Bryden, H.L., Kinder, T.H., 1991. Steady two-layer exchange through the Strait of Gibraltar. *Deep-Sea Research* 38 (1), S445–S463.

- Buccheri, G., Capretto, G., Di Donato, V., Esposito, P., Ferruzza, G., Pescatore, T.S., Russo Ermolli, E., Senatore, M.R., Sprovieri, M., Bertoldo, M., Carella, D., Madonia, G., 2002. A high resolution record of the last deglaciation in the southern Tyrrhenian Sea: environmental and climatic evolution. *Marine Geology* 186, 447–470.
- Cacho, I., Grimalt, J.O., Pelejero, C., Canals, M., Sierro, F.J., Flores, J.A., Shackleton, N., 1999. Dansgaard-Oeschger and Heinrich event imprints in Alboran Sea paleotemperatures. *Paleoceanography* 14 (6), 698–705.
- Cacho, I., Grimalt, J.O., Sierro, F.J., Shackleton, N.J., Canals, M., 2000. Evidence for enhanced Mediterranean thermohaline circulation during rapid climate coolings. *Earth and Planetary Science Letters* 183, 417–429.
- Cacho, I., Grimalt, J.O., Canals, M., Sbaiff, L., Shackleton, N.J., Schönfeld, J., Zahn, R., 2001. Variability of the western Mediterranean Sea surface temperature during the last 25,000 years and its connection with the Northern Hemisphere climatic changes. *Paleoceanography* 16, 40–52.
- Capotondi, L., Borsetti, A.M., Morigi, C., 1999. Foraminiferal eco-biozones, a high resolution proxy for the late Quaternary biochronology in the central Mediterranean. *Marine Geology* 153, 253–274.
- Casford, J.S.L., Rohling, E.J., Abu-Zied, R., Cooke, S., Fontanier, C., Leng, M., Lyskousis, V., 2002. Circulation changes and nutrient concentrations in the late Quaternary Aegean Sea: a nonsteady state concept for sapropel formation. *Paleoceanography* 17, 1–11.
- Comboureu Nebout, N., Turon, J.L., Zahn, R., Capotondi, L., Londeix, L., Pahnke, K., 2002. Enhanced aridity and atmospheric high-pressure stability over the western Mediterranean during the North Atlantic cold events of the past 50 kyr. *Geology* 30, 863–866.
- Curry, W.B., Shackleton, N.J., Richter, C., Bralower, T.J., 1995. Shipboard Scientific Party. In: *Proceedings of the Ocean Drilling Program, Initial Reports*, 154, College Station, TX, Ocean Drilling Program, 1111pp.
- Damuth, J.E., Flood, R.D., 1984. Morphology, sedimentation processes, and growth pattern of the Amazon Deep-Sea fan. *Geo-Marine Letters* 3 (2–4), 109–117.
- Dansgaard, W., Johnsen, S.J., Clausen, H.B., Dahl-Jensen, D., Gundestrup, N.S., Hammer, C.V., Hvidberg, C.S., Steffensen, J.P., Sveinbjornsdottir, A.E., Jouzel, J., Bard, G., 1993. Evidence for general instability of past climate from a 250 kyr ice-core record. *Nature* 364, 218–220.
- Deamer, G.A., Kodama, K.P., 1990. Compaction-induced inclination shallowing in synthetic and natural clay-rich sediments. *Journal of Geophysical Research* 95, 4511–4529.
- Ducassou, E., Capotondi, L., Murat, A., Bernasconi, S., Mulder, T., Gonthier, E., Migeon, S., Duprat, J., Giraudeau, J., Mascle, J., 2007. Multiproxy Late Quaternary stratigraphy of the Nile deep-sea turbidite system—towards a chronology of deep-sea terrigenous systems. *Sedimentary Geology* 200 (1–2), 1–13.
- Emeis, K.C., Emeis, H., Schulz, U., Struck, M., Rossignol-Strick, H., Erlenkeuser, M.W., Howell, D., Kroon, A., Mackensen, S., Ishizuka, T., Oba, T., Sakamoto, I., Koizumi, I., 2003. Eastern Mediterranean surface water temperatures and $\delta^{18}\text{O}$ composition during deposition of sapropels in the late Quaternary. *Paleoceanography* 18, 1–18.
- GEBCO, 1997. General Bathymetric Chart of the Oceans, British Oceanographic Data Centre, British Cartographic Data Centre, <http://www.bodc.ac.uk/projects/international/gebco/>.
- Geraga, M., Tsaila-Monopolis, S., Ioakim, C., Papatheodorou, G., Ferentinos, G., 2005. Short-term climate changes in the southern Aegean Sea over the last 48,000 years. *Palaeogeography, Palaeoclimatology, Palaeoecology* 220, 311–332.
- GRIP members, 1993. Greenland Ice-Core Project (GRIP) members, Climate instability during the last interglacial period recorded in the GRIP ice core. *Nature* 364, 203–207.
- Guyodo, Y., Channell, J.E.T., Thomas Ray, G., 2002. Deconvolution of u-channel paleomagnetic data near geomagnetic reversals and short events. *Geophysical Research Letters* 29 (17), 1845.
- Hemleben, C., Spindler, M., Anderson, O.R., 1989. *Modern Planktonic Foraminifera*. Springer, New York (pp. 1–363).
- Heinrich, H., 1988. Origin and consequences of cyclic ice rafting in the Northeast Atlantic Ocean during the past 130,000 years. *Quaternary Research* 29, 142–152.
- Hilgen, F.J., 1991a. Astronomical calibration of Gauss to Matuyama sapropels in the Mediterranean and implication for the geomagnetic polarity timescale. *Earth Planetary Science Letters* 104, 226–244.
- Hilgen, F.J., 1991b. Extension of the astronomically calibrated (polarity) timescale to the Miocene–Pliocene boundary. *Earth Planetary Science Letters* 107, 349–368.
- Hilgen, F.J., Krijgsman, W., 1999. Cyclostratigraphy and astrochronology of the Tripoli diatomite Formation (pre-evaporite Messinian Sicily, Italy). *Terra Nova* 11, 16–22.
- Hilgen, F.J., Abdul Aziz, H., Krijgsman, W., Langereis, C.G., Lourens, L.J., Meulenkamp, J.E., Raffi, I., Steenbrink, J., Turco, E., van Vugt, N., Wijbrans, J.R., Zachariasse, W.J., 1999. Present status of the astronomical (polarity) time-scale for the Mediterranean Late Neogene. *Philosophical Transactions of the Royal Society of London Series A (The Royal Society)* 357, 1931–1947.
- Hilgen, F.J., Abdul Aziz, H., Krijgsman, W., Raffi, I., Turco, E., 2003. Integrated stratigraphy and astronomical tuning of the Serravallian and lower Tortonian at Monte dei Corvi (Middle–Upper Miocene, northern Italy). *Palaeogeography, Palaeoclimatology, Palaeoecology* 199, 229–264.
- Imbrie, J., Hays, J.D., Martinson, D.G., McIntyre, A., Mix, A.C., Morley, J.J., Pisias, N.G., Prell, W.L., Shackleton, N.J., 1984. The orbital theory of Pleistocene climate: support from a revised chronology of the marine $\delta^{18}\text{O}$ record. In: Berger, A.L., et al. (Eds.), *Milankovitch and Climate*, Part I. Reidel, Dordrecht, pp. 269–305.
- Iorio, M., Sagnotti, L., Angelino, A., Budillon, F., D'Argenio, B., Dinare's-Turell, J., Macri, P., Marsella, E., 2004. High-resolution petrophysical and palaeomagnetic study of late-Holocene shelf sediments, Salerno Gulf, Tyrrhenian Sea. *The Holocene* 14 (3), 426–435.
- Jorissen, F.J., Asioli, A., Borsetti, A.M., de Visser, L., Hilgen, F.J., Rohling, E.J., van der Borg, K., Vergnaud-Grazzini, C., Zachariasse, W.J., 1993. Late Quaternary central Mediterranean biochronology. *Marine Micropaleontology* 21, 169–189.
- Kenyon, N.H., Klauke, I., Millington, J., Ivanov, M.K., 2002. Sandy submarine canyon-mouth lobes on the western margin of Corsica and Sardinia, Mediterranean Sea. *Marine Geology* 184, 69–84.
- Kirschvink, J.L., 1980. The least-square line and plane and the analysis of paleomagnetic data. *Geophysical Journal of the Royal Astronomical Society* 62, 699–718.
- Laskar, M., Gastineau, F., Joutel, B., Levrard, P., Robutel, 2004. A new astronomical solution for the long term evolution of the insolation quantities of Mars. *Lunar and Planetary Science XXXV*, 1–2.
- Lourens, L.J., 2004. Revised tuning of Ocean Drilling Program Site 964 and KC01B (Mediterranean) and implication for the $\delta^{18}\text{O}$, tephra, calcareous nannofossil, and geomagnetic reversal chronologies of the past 1.1 Myr. *Paleoceanography* 19, 3010.
- Lourens, L.J., Hilgen, F.J., Zachariasse, W.J., Van Hoof, A.A.M., Antonarakou, A., Vergnaud-Grazzini, C., 1996a. Evaluation of the Plio-Pleistocene astronomical time scale. *Paleoceanography* 11, 391–413.
- Lourens, L.J., Hilgen, F.J., Raffi, I., Vergnaud-Grazzini, C., 1996b. Early Pleistocene chronology of the Vrica section (Calabria, Italy). *Paleoceanography* 11, 797–812.
- Lourens, L.J., Hilgen, F.J., Raffi, I., 1998. Base of large Gephyrocapsa and astronomical calibration of Early Pleistocene sapropels in site 967 and hole 969D: solving the chronology problem of the Vrica section (Calabria, Italy). In: Robertson, A.H.F., Emeis, K.C., Richter, C., Camerlinghi, A. (Eds.), *Proceedings of the ODP, Scientific Results*, vol. 160, pp. 191–197.
- Lund, S., Stoner, J.S., Channell, J.E.T., Acton, G., 2006. A summary of Brunhes paleomagnetic field variability recorded in Ocean Drilling Program cores. *Physics of the Earth and Planetary Interiors* 156, 194–204.
- Masclé, G.H., Tricart, P., Bouillin, J.P., Compagnoni, R., Depardon, S., Masclé, J., Pecher, A., Peis, D., Rekhiss, F., Rolfo, F., Torelli, L., 2001a. Données de campagne des plongées Cyana Sarcya-Sartucya. In: Masclé, G., Tricart, P. (Eds.), *Le Canal de Sardaigne: les plongées Cyana*, Vol. 34. *Geologie Alpine*, Mém. H.S., pp. 7–113.
- Masclé, G.H., Tricart, P., Torelli, L., Bouillin, J.P., Rolfo, F., Lapiere, H., Monié, P., Depardon, S., Masclé, J., Peis, D., 2001b. Evolution of the Sardinia Channel (Western Mediterranean): new constraints from a diving survey on Cornacya seamount off SE Sardinia. *Marine Geology* 179 (3–4), 179–201.
- Masclé, G.H., Tricart, P., Torelli, L., Bouillin, J.P., Compagnoni, R., Depardon, S., Masclé, J., Pecher, A., Peis, D., Rekhiss, F., Rolfo, F., Bellon, H., Brocard, G., Lapiere, H., Monié, P., Poupeau, G., 2004. Structure of the Sardinia Channel: crustal thinning and tardi-orogenic extension in the Apenninic-Maghrebien orogen; results of the Cyana submersible survey (SARCYA and SARTUCYA) in the Western Mediterranean. *Bulletin de la Société Géologique de France* 175 (6), 607–627.
- Millot, C., 1987. Circulation in the western Mediterranean Sea. *Oceanology Acta* 10, 143–149.
- Moreno, A., Cacho, I., Canals, M., Prins, M.A., Sanchez-Goni, M.-F., Grimalt, J.O., Weltje, G.J., 2002. Saharan dust transport and high latitude glacial climatic variability: the Alboran Sea record. *Quaternary Research* 58, 318–328.
- Mutti, E., Tinterri, R., Remacha, E., Mavilla, N., Angella, L., 1999. An Introduction to the Analysis of Ancient Turbidite Basins From an Outcrop Perspective, Continuing Education Course Note Series, vol. 39. American Association Petroleum Geologists, Tulsa, OK.
- NGRIP Members, 2004. High-resolution record of Northern Hemisphere climate extending into the last interglacial period. *Nature* 431, 147–151.
- Narcisi, B., Vezzoli, L., 1999. Quaternary stratigraphy of distal tephra layers in the Mediterranean—an overview. *Global Planetary Change* 21, 31–50.
- Normark, W.R., Barnes, N.E., Coumes, F., 1984. Rhone deep-sea fan: a review. *Geo-Marine Letters* 3 (2–4), 155–160.
- Normark, W.R., Piper, D.J.W., Hiscott, R.N., 1998. Sea level control on the textural characteristics and depositional architecture of the Hueneme and associated fan systems, Santa Monica Basin, California. *Sedimentology* 26, 749–774.
- Oda, H., Shibuya, H., 1996. Deconvolution of long-core paleomagnetic data of Ocean Drilling Program by Akaike's Bayesian information criterion minimization. *Journal of Geophysical Research* 101, 2815–2834.
- Palike, H., Frazier, J., Zachos, J.C., 2006. Extended orbitally forced paleoclimatic records from the equatorial Atlantic Ceara Rise. *Quaternary Science Reviews* 25, 3138–3149.
- Passariello, I., Marzaioli, F., Lubritto, C., Rubino, M., D'Onofrio, A., De Cesare, N., Borriello, G., Casa, G., Palmieri, A., Rogalla, D., Sabbarese, C., Terrasi, F., 2007. Radiocarbon sample preparation at the Circe AMS laboratory in Caserta. *Italy Radiocarbon* 49 (2), 225–232.
- Pérez-Folgado, M., Sierro, F.J., Flores, J.A., Cacho, I., Grimalt, J.O., Zahn, R., Shackleton, N., 2003. Western Mediterranean planktonic foraminifera events and millennial climatic variability during the last 70 kyr. *Marine Micropaleontology* 48 (1–2), 49–70.
- Pérez-Folgado, M., Sierro, F.J., Flores, J.A., Grimalt, J.O., Zahn, R., 2004. Paleoclimatic variations in foraminifer assemblages from the Alboran Sea (Western Mediterranean) during the last 150 ka in ODP Site 977. *Marine Geology* 212, 113–131.

- Peterson, L.C., Haug, G.H., Hughen, K.A., Rohl, U., 2000. Rapid changes in the hydrologic cycle of the tropical Atlantic during the Last Glacial. *Science* 290, 1947–1951.
- Pinardi, N., Masetti, E., 2000. Variability of the large scale general circulation of the Mediterranean Sea from observations and modelling: a review. *Palaeogeography, Palaeoclimatology, Palaeoecology* 158, 153–173.
- Principato, M.S., Giunta, S., Corselli, C., Negri, A., 2003. Late Pleistocene–Holocene planktonic assemblages in three box-cores from the Mediterranean ridge area (west–southwest of Crete): palaeoecological and palaeoceanographic reconstruction of sapropel S1 interval. *Palaeogeography, Palaeoclimatology, Palaeoecology* 190, 61–77.
- Prins, M.A., Postma, G., Cleveringa, J., Cramp, A., Kenyon, N.H., 2000. Controls on terrigenous supply to the Arabian Sea during the Late Quaternary: the Indus Fan. *Marine Geology* 169, 327–349.
- Pujol, C., Vergnaud-Grazzini, C., 1995. Distribution patterns of live planktonic foraminifers as related to regional hydrography and productive system of the Mediterranean Sea. *Marine Micropaleontology* 25, 187–217.
- Reading, H.G., Richards, M.T., 1994. The classification of deep-water siliciclastic depositional systems by grain size and feeder system. *American Association Petroleum Geologists Bulletin* 78, 792–822.
- Richards, M., Bowman, M., Reading, H., 1998. Submarine-fan systems. I: Characterization and stratigraphic prediction. *Marine and Petroleum Geology* 15 (7), 671–689.
- Roberts, A.P., Winkhofer, M., 2004. Why are geomagnetic excursions not always recorded in sediments? Constraints from post-depositional remanent magnetization lock-in modelling. *Earth and Planetary Science Letters* 227 (3–4), 345–359.
- Rohling, E.J., Hayes, A., Kroon, D., De Rijk, S., Zachariasse, W.J., Eisma, D., 1998. Abrupt cold spells in the NW Mediterranean. *Paleoceanography* 13, 316–322.
- Rohling, E.J., Cane, T.R., Cooke, S., Sprovieri, M., Boulabassi, I., Emeis, K.C., Schiebel, R., Kroon, D., Jorissen, F.J., Lorré, A., Kemp, A.E.S., 2002. African monsoon variability during the previous interglacial maximum. *Earth and Planetary Science Letters* 202, 61–75.
- Rohling, E.J., Mayewski, P.A., Challenor, P., 2003. On the timing and mechanism of millennial-scale climate variability during the last glacial cycle. *Climate Dynamics* 20, 257–267.
- Sagnotti, L., Budillon, F., Dinarès-Turell, J., Iorio, M., Macrí, P., 2005. Evidence for a variable paleomagnetic lock-in depth in the Holocene sequence from the Salerno Gulf (Italy): implications for “high-resolution” paleomagnetic dating. *Geochemistry, Geophysics, and Geosystems* 6 (11), 1–11.
- Sangiorgi, F., Dinelli, E., Maffioli, P., Capotondi, L., Giunta, S., Morigi, C., Principato, M.S., Negri, A., Emeis, K.C., Corselli, C., 2006. Geochemical and micropaleontological characterisation of a Mediterranean sapropel S5: a case study from core BAN89GC09 (south of Crete). *Palaeogeography, Palaeoclimatology, Palaeoecology* 235, 192–207.
- Sanvoisin, R., D’Onofrio, S., Lucchi, R., Violanti, D., Castradori, D., 1993. 1Ma Paleoclimatic record from the Eastern Mediterranean-Marflux Project: the first results of micropaleontological and sedimentological investigation of a long piston core from the Calabrian Ridge. *Il Quaternario* 6, 169–188.
- Sartori, R., Carrara, G., Torelli, L., Zitellini, N., 2001. Neogene evolution of the southwestern Tyrrhenian Sea (Sardinia Basin and western Bathyal plain). *Marine Geology* 1–4 (175), 47–66.
- Sbaffi, L., Wezel, F.C., Curzi, G., Zoppi, U., 2004. Millennial- to centennial-scale palaeoclimatic variations during Termination I and the Holocene in the central Mediterranean Sea. *Global and Planetary Change* 40, 201–217.
- Sprovieri, R., 1991. Plio-Pleistocene paleoclimatic evolution at ODP Leg 107 Site 653 (Tyrrhenian Sea, Western Mediterranean). *Memorie della Società Geologica Italiana* 44, 135–144.
- Sprovieri, R., Di Stefano, E., Incarbona, A., Gargano, M.E., 2003. A high-resolution of the last deglaciation in the Sicily Channel based on foraminiferal and calcareous nannofossil quantitative distribution. *Palaeogeography, Palaeoclimatology, Palaeoecology* 202, 119–142.
- Sprovieri, R., Di Stefano, E., Incarbona, A., Oppo, D.W., 2006. Suborbital climate variability during Marine Isotopic Stage 5 in the central Mediterranean basin: evidence from calcareous plankton record. *Quaternary Science Reviews* 25, 2332–2342.
- Stuiver, M., Reimer, P.J., 1993. Extended ^{14}C data base and revised CALIB 3.0 ^{14}C Age calibration program. *Radiocarbon* 35 (1), 215–230.
- Tan, X., Kodama, K.P., 2003. An analytical solution for correcting palaeomagnetic inclination error. *Geophysical Journal International* 152 (1), 228–236.
- Tan, X., Kodama, K.P., Lin, H., Fang, D., Sun, D., Li, Y., 2003. Palaeomagnetism and magnetic anisotropy of Cretaceous red beds from the Tarim basin, northwest China: evidence for a rock magnetic cause of anomalously shallow palaeomagnetic inclinations from central Asia. *Journal of Geophysical Research* 108 (B2), 2107.
- Tauxe, L., Kent, D.V., 1984. Properties of a detrital remanence carried by hematite from study of modern river deposits and laboratory redeposition experiments. *Geophysical Journal of the Royal Astronomical Society* 77, 543–561.
- Tauxe, L., Kent, D.V., 2004. A simplified statistical model for the geomagnetic field and the detection of shallow bias in paleomagnetic inclinations: was the ancient magnetic field dipolar? In: Channell, J.E.T., et al. (Eds.), *Timescales of the Paleomagnetic field*, vol. 145. *Geophysical Monograph*, pp. 101–116.
- Walker, R.G., 1967. Turbidite sedimentary structures and their relationship to proximal and distal depositional environments. *Journal of Sedimentary Petrology* 37 (1), 25–37.
- Walker, R.G., 1992. Turbidites and submarine fans. In: Walker, R.G., James, N.P. (Eds.), *Facies Model Response to Sea-level Change*. Geological Association of Canada, Ontario, pp. 239–263.
- Waelbroeck, C., Labeyrie, L., Michel, E., Duplessy, J.C., Lambeck, K., McManus, J.F., Balbon, E., Labracherie, M., 2002. Sea-level and deep water temperature changes derived from benthic foraminifera isotopic records. *Quaternary Science Reviews* 21, 295–305.
- Watkins, J.M., Mix, A.C., Wilson, J., 1996. Living planktic foraminifera: tracers of circulation and productivity regimes in the central equatorial Pacific. *Deep-Sea Research II* 43, 1257–1282.
- Wolf-Welling, T.C.W., Cowan, E.A., Daniels, J., Eyles, N., Maldonado, A., Pudsey, C.J., 2001. Diffuse spectral reflectance data from rise Sites 1095, 1096, 1101 and Palmer Deep Sites 1098 and 1099 (Leg 178, Western Antarctic Peninsula). In: Barker, P.F., Camerlenghi, A., Acton, G.D., Ramsay, A.T.S. (Eds.), *Proceeding Ocean Drilling Program, Scientific Results*, vol. 178, pp. 1–22.
- Zaric, S., Donner, B., Fischer, G., Mulitza, S., Wefer, G., 2005. Sensitivity of planktic foraminifera to sea surface temperature and export production as derived from sediment trap data. *Marine Micropaleontology* 55, 75–105.